Research Article: Open Access

VIBGYOR ePress

International Journal of
Magnetics and Electromagnetism

# Optimization of the Absorption of Radiation in NiZnMn Ferrite by Electron-Phonons in Composites of Dielectric Polymer and Crystals

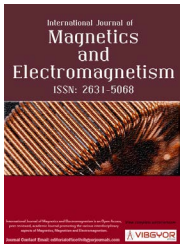

ISSN: 2631-5068

***Régia C Pessoa[1], Ricardo S Nasar[2*], Marinalva C Nasar[2] and José H Araújo[3]***

[1]*Chemistry Department, State University of Roraima, Boa Vista, Brazil*

[2]*Institute of Chemistry, Federal University of Rio Grande do Norte, Natal, Brazil*

[3]*Department of Theoretical and Experimental Physic, Federal University of Rio Grande do Norte, Natal, Brazil*

**Abstract**

Ferrites were synthesized with the formula $Ni_{0.5-x}Zn_{0.5}Mn_xFe_2O_4$ for x = 0, 0.3, and 0.5 mol%, respectively. The magnetic characteristics and the absorption of radiation of the powder-epoxy composite were investigated. X-ray diffractometry, XRD and scanning electron microscopy, SEM, were performed. The magnetic hysteresis was investigated by vibrating-sample magnetometer, VSM, and the Bohr magneton was compared with the reflectivity measurements of the composites. The Bohr magneton of 6 μB/cell for NiZn and 7.5 μB/cell for NiZnMn, respectively, show the effect of inversion between theoretical and experimental results. The NiZn reached reflectivity of -16 dB at 8 GHz with 98% of radiation absorption. Preliminary analysis indicates that electronic mobility into the crystals and phonons (vibrational modes) of the structure with a more efficient epoxy polymer in heat dissipation are the preponderant causes of propagation and dissipation of magnetic waves into the composite. These indicate that high tendency to magnetization is not only one cause of the absorption of radiation.

**Keywords**

Absorbing materials, Ferrites, Magnetism, Phonons

## Introduction

The nanometric ferrites represent a class of ceramic magnetic materials with wide application in electromagnetic devices due to their electrical and magnetic characteristics [1-7]. The general formula for these ferrites is $MFe_2O_4$, wherein M is one or more divalent metal ions such as $Ni^{2+}$, $Cu^{2+}$, $Mg^{2+}$, $Mn^{2+}$, $Zn^{2+}$, and others. Among these materials, ferrites based on NiZn, NiCuZn, MnZn and MgNi have's spinel type structures and have high scientific and technological interest because of their applications in the electronics industry as magnetic high resistivity devices [8-10]. The spinels include a broad category of compounds employed in several areas and for specific purposes, such as ferroelectric, insulators and superconductors [11,12]. Preparation of polycrystalline ferrites with very good magnetic properties generally requires the use of synthesis via wet or by combustion process [13-16], as the main problem lies in the

***Corresponding author:** *Ricardo S Nasar, Institute of Chemistry, Federal University of Rio Grande do Norte, Natal, Brazil*

**Accepted:** January 28, 2019; **Published:** January 30, 2019



ISSN 2631-5068

9 772631 506008

Pessoa et al. Int J Magnetics Electromagnetism 2019, 5:017

**Citation:** Pessoa RC, Nasar RS, Nasar MC, Araújo JH (2019) Optimization of the Absorption of Radiation in NiZnMn Ferrite by Electron-Phonons in Composites of Dielectric Polymer and Crystals. Int J Magnetics Electromagnetism 5:017

fact that many of the properties required for the applications are not intrinsic but extrinsic [17,18]. Thus, the ferrites are not defined by their chemical composition and crystalline structure, but instead also requires knowledge and parameters that control their microstructure, such as density, grain size, porosity, excess oxygen, and their intra- and inter-granular distribution [19,20].

In industrial scale the nanoferrites are prepared by the conventional ceramic method, which comes from the mixture of oxides in high-energy mills. Most of the resulting products are not stoichiometric and homogeneous in a microscopic scale, since the compounds have already been defined and the crystallographic phase can lead to final product phases that do not react. Thus, the properties are often not reproducible.

Thus, it is well known that the properties of ferrites are strongly influenced by the composition and the preparation method used in their synthesis. In the laboratory, many current methods, such as the technique of pyrolysis, sol-gel, coprecipitation and combustion method have been adopted for the synthesis using metal nitrates [21-24].

At present, there is a great emphasis on the study of electromagnetic radiation absorbing materials, RAM, applied to aerospace industry and electronics [25]. In the state of the art, the purpose is to develop materials for protection of electronic or optical devices used in aerospace (rockets and satellites) and mobile telephony. In this context, RAMs of composites ferrites/polymers based on ferrites with different additives [26] mixed with epoxy, acrylates and carbon fibers are investigated [27]. Other materials used are based on polyaniline (PANI) embedded into a polyurethane matrix [28], polyvinylchloride (PVC) matrix or polychloroprene vulcanized [29].

In this work we used the process of citrate precursors based on the Pechini method [30]. Samples of NiZn, NiZnMn and MnZn were prepared with $Ni_{0.5-x}Zn_{0.5}Mn_xFe_2O_4$ as the general formula. The work consists of a behavioral analysis between theoretical data calculated using experimental data in analyzing and the influence of polymer-crystal on the absorption of electromagnetic radiation in nanoferrites.

## Experimental Procedure

Ferrite were synthesized, using the citrates precursor method in the overall composition $Ni_{0.5-x}Zn_{0.5}Mn_xFe_2O_4$, for x = 0 (A-I), 0.3 (A-II), 0.5 (A-III), respectively. The materials used were: citric acid; $C_6H_8O_7$ (99.5% Vetec), nickel nitrate; $Ni(NO_3)_2{\cdot}6H_2O$ (99.5% Aldrich), zinc nitrate; $Zn(NO_3)_2{\cdot}6H_2O$ (99.5% Aldrich), manganese nitrate; $Mn(NO_3)_2{\cdot}6H_2O$ (99.5% Aldrich) and iron nitrate; $Fe(NO_3)_2{\cdot}9H_2O$ (99% Aldrich).

Citric acid was mixed proportional to the mass of metal (2:1) in water in the ratio of 50/50 vol% citric acid-nitrate/water. The solutions were heated at 70 °C for 6 hours. The citrates were mixed stoichiometrically in magnetic mixer according to the before above-mentioned formula. Mixtures of citrates were heated at 85 °C for 10 hours. The resins were packed in beckeres and heated in a muffle EDG type (P-S 3) at 350 °C for 3 hours. The powders were deagglomerated in an agate mortar and sieved in an ABNT (ASTM) 325 mesh. One batch of each powder was calcined at 1100 °C for 3 hours. The powders were analyzed by X-ray equipment using a Shimadzu XRD 6000 diffractometer with, a tube voltage of 30 kV, tube current of 30 mA with CuKα radiation (λ = 1.5418 Å), and an angle 2θ step = 2°/min. (15° and 85°). A Shimadzu graphite monochromator D/tex ultra was used. The XRD pattern were analyzed by Rietveld refinement with using the MAUD software v. 2044 version. A Scanning electron microscopy (SEM) was made performed in equipment Philips XL-30-ESEM. The Vibrating sample magnetometry (VSM) was taken in a LMMM equipment for measuring MxT in the temperature range of -196 °C to 377 °C. The analysis of reflectivity was made in an apparatus using waveguide type by IAE/DCTA within a range of 8.2-12.4 GHz. Direction coupler (X752C model-HP) was used to measure the reflected energy of the samples. A synthesized seeper (83752A model-Agilent) is connected by a cable to the coaxial adapter, and the spectrum analyzer (70000 model-HP) is wired in the coaxial adapter of the signal output. The transmitted energy is absorbed, the reflected energy is read in the spectrum analyzer. The reflection coefficient is determined relative to a reading obtained from the sample and from a polished metal plate of intense reflection. The composites were prepared by mixing epoxy resin (Araldit LY 556, $C_{18}H_{21}ClO_3$, based on bisphenol-A) and packed into molds. The plates with composites were supported on a metal plate with 100% reflectivity. The mixture of resin/

ferrite was weighted in ratio of 50/50. To estimate the obtained experimental values in terms of the Bohr magneton, $\mu_B$ [31], the following equation was applied:

$$M = (Pm.Ms)/(N.\beta) \quad (1)$$

Where $M$ is the magnetization in Bohr magneton per unit cell, $Pm$ is the atomic weight, $Ms$ is the saturation magnetization, $N$ is the Avogadro number, and $\beta$ is the conversion factor for expressing the magnetic moment per unit cell, which is equal to $9.27 \times 10^{-21}$ erg/Gauss.

## Results and Discussions

Figure 1 shows the X-ray diffraction, XRD pattern of the A-I, A-II and A-III samples calcined at 1100 °C/3h. The A-II composition do not showed hematite, while the samples A-I and A-III showed 5% and 12%, respectively.

Increasing calcination temperature favors the formation of single phase for ferrite with manganese, whereas the spinel crystalline lattice has more stability above a temperature of 1000 °C. Temperatures above 1200 °C favor the formation

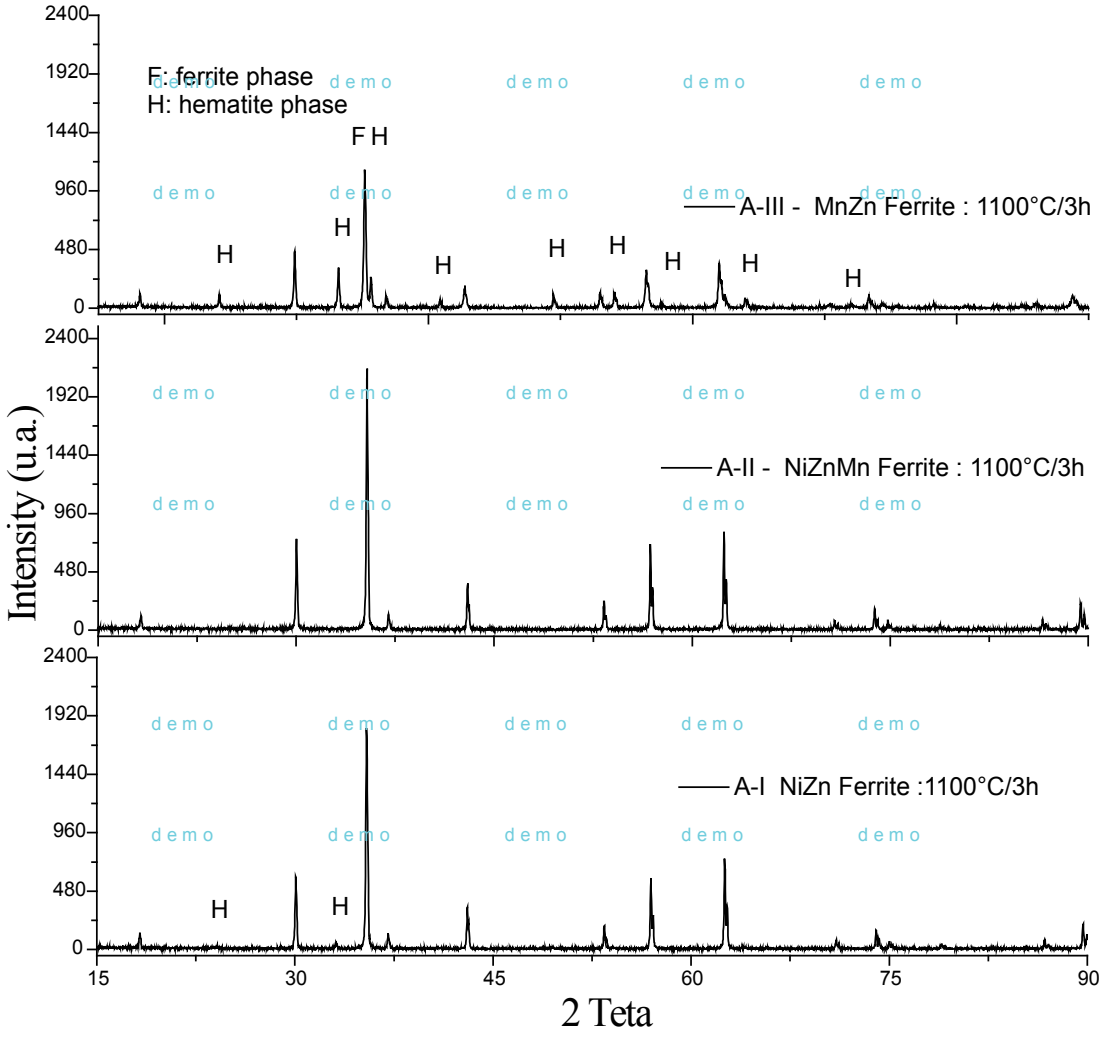


**Figure 1:** X-ray diffractogram pattern of the A-I, A-II and A-III ferrites compositions calcineds at 1100 °C/3h.

**Table 1:** Refinement by Rietveld of A-I, A-II and A-III ferrites calcineds at 1100 °C/3h.

| | Phase | % of Phase | Lat. Par. (a)(Å) | Cs (µm) | Rw | Sig |
|---|---|---|---|---|---|---|
| A-I | NiZn Ferrite | 95 ± 2.1 | 8.39 | 1.03 ± 0.08 | 26.16 | 1.22 |
| | Hematite | 5.0 ± 0.2 | 5.43 | 0.54 ± 0.06 | | |
| A-II | NiZnMn Ferrite | 100 | 8.41 | 0.61 ± 0.03 | 26.05 | 1.25 |
| A-III | MnZn Ferrite | 88 ± 1.3 | 8.45 | 1.14 ± 0.10 | 29.51 | 1.32 |
| | Hematite | 12 ± 0.32 | 5.42 | 0.49 ± 0.05 | | |

of a ferrite single phase, thus, it was obtained a decreasing of hematite phase in the A-II and A-III samples. Table 1 shows the refinement by Rietveld of samples calcined at 1100 °C/3h with average crystallite sizes of ferrite phase of 1.03 µm (A-I), 0.61 µm (A-II) and 1.14 µm in (A-III). Generally, in this temperature the average crystallite sizes are of the order of more of 1 µm. In Figure 2, the XRDs of the calcined powders at 350 °C/3h and analyzed by Rietveld refinement are shown. The analysis

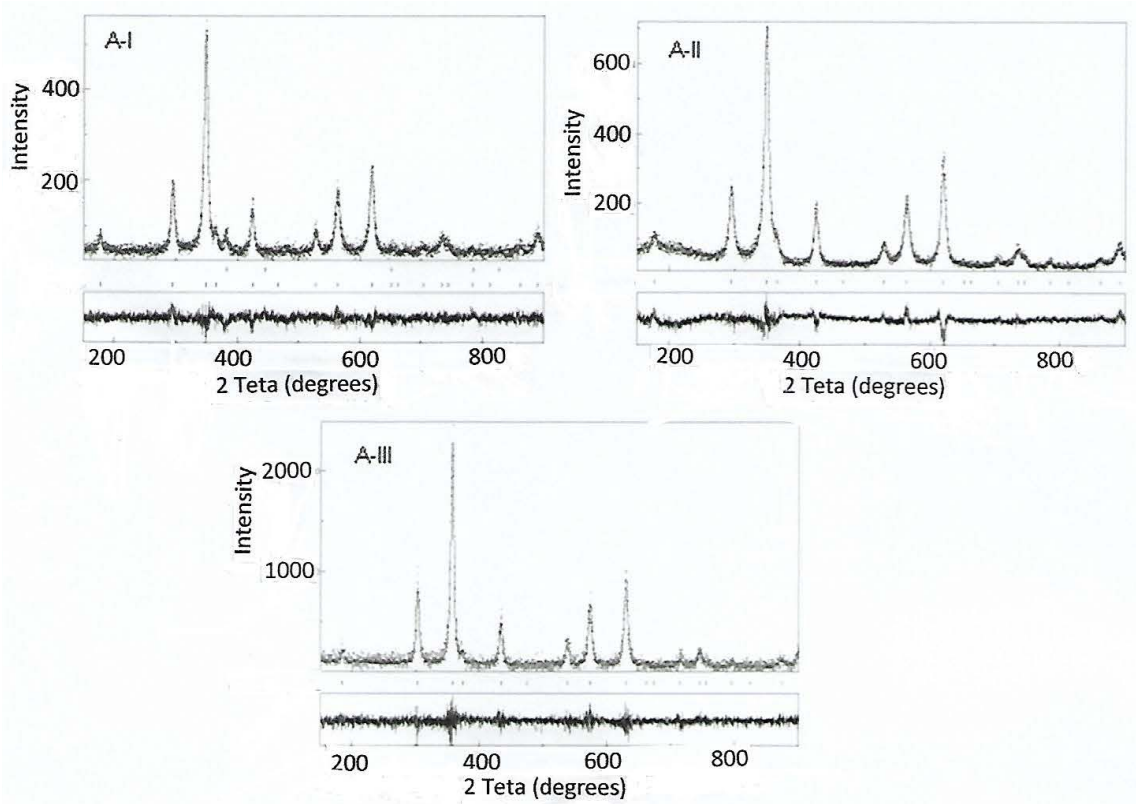


**Figure 2:** X-ray diffraction pattern of the A-I, A-II and A-III ferrites compositions calcineds at 350 °C/3h.

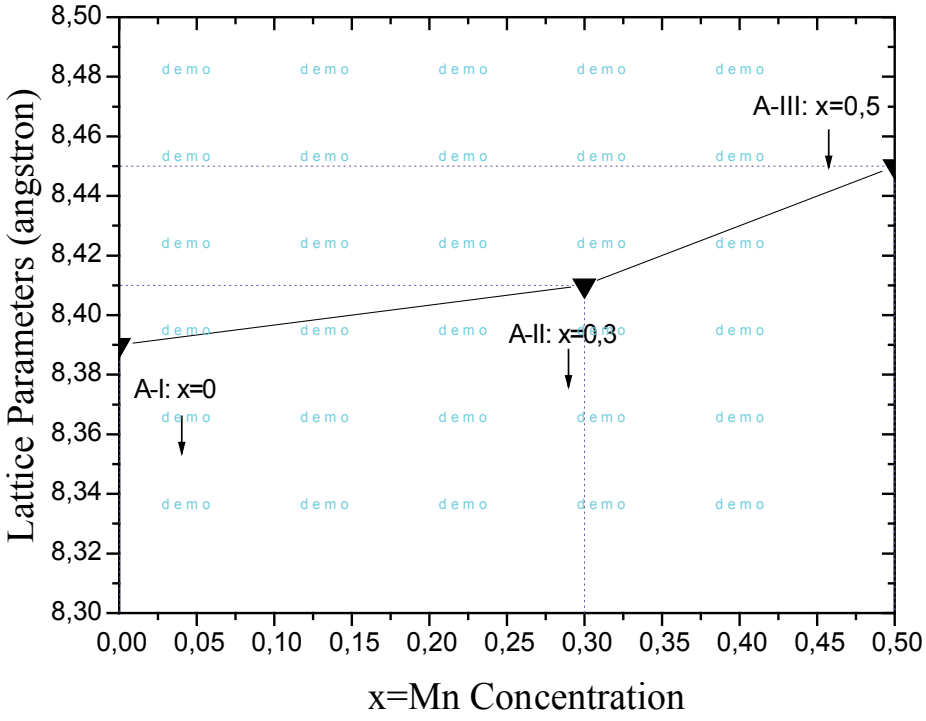


**Figure 3:** Lattice parameters (a), depending on the compositions of $Ni_{0.5-x}Zn_{0.5}Mn_xFe_2O_4$ ferrites.

**Citation:** Pessoa RC, Nasar RS, Nasar MC, Araújo JH (2019) Optimization of the Absorption of Radiation in NiZnMn Ferrite by Electron-Phonons in Composites of Dielectric Polymer and Crystals. Int J Magnetics Electromagnetism 5:017

showed the formation of a single phase of the spinel ferrite type.

The structural parameters indicate that the synthesized ferrites crystallize in the cubic structure with space group Fd-3m:1. The data indicate that ferrites have an inverse spinel structure. All the divalent metal ions, such as $Ni^{2+}$ and $Mn^{2+}$, would occupy tetrahedral positions (normal spinel), but these not happening demonstrating that divalent metals occupy both tetrahedral and octahedral positions (inverse spinel).

The analysis of the lattice parameters with the concentration of Mn, Figure 3, shows that the parameter increases linearly with by increasing of x

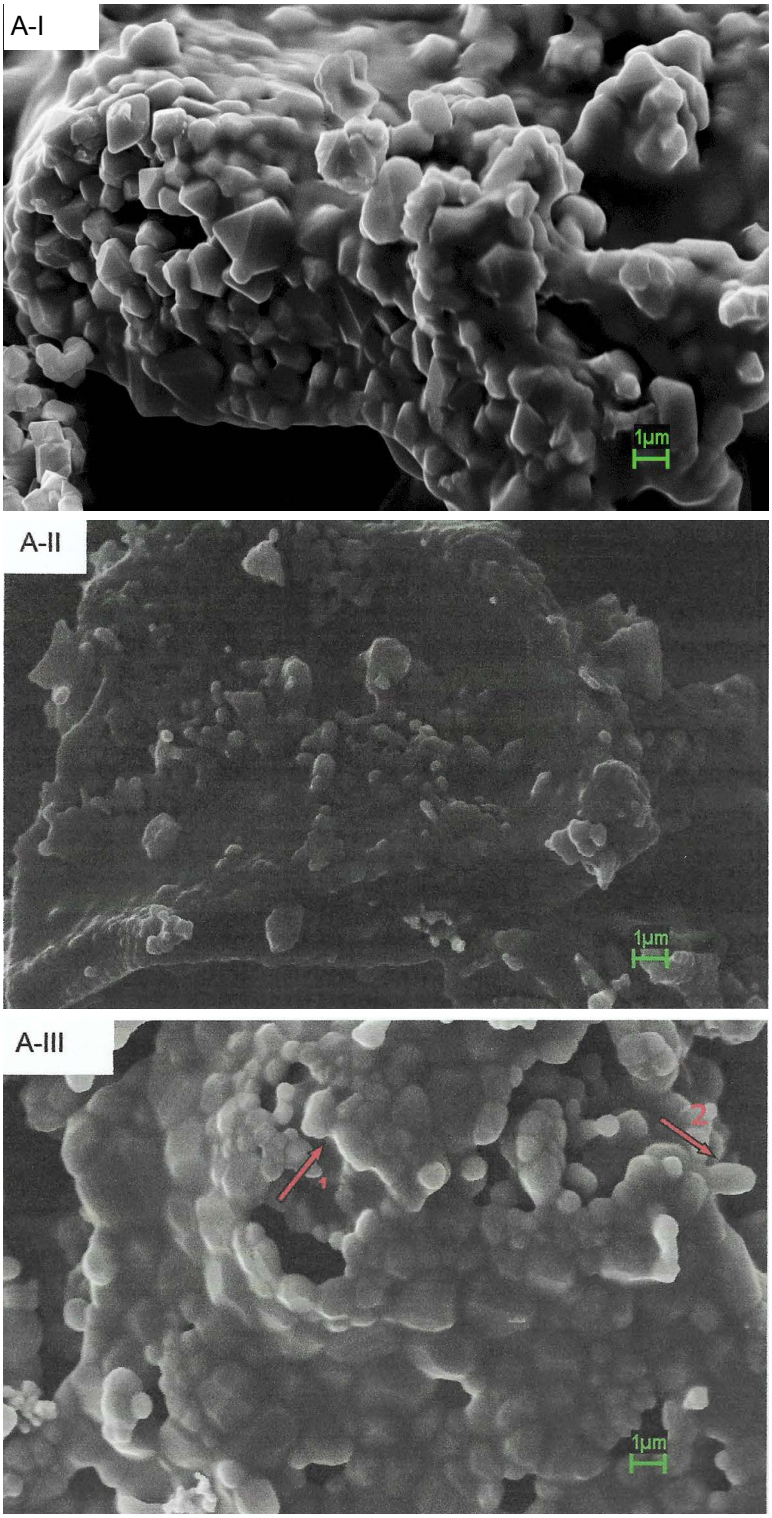


**Figure 4:** Scanning electron microscopy, SEM of ferrites, a) NiZn (A-I); b) NiZnMn (A-II); c) MnZn (A-III); calcineds at 1100 °C/3 h.

concentration. This occurs because the $Mn^{2+}$ (0.82Å) ion has larger ionic radius than the $Ni^{2+}$ (0.69Å) and $Zn^{2+}$ (0.74Å) ions. This clearly shows the diffusion effect of manganese on the ferrite structure. Rezlescu, et al. [6] studied the effect of the addition of divalent ions on the NiZn ferrite and obtained lattice parameter of 8.39Å. The compositions AII and AIII obtained 8.41Å and 8.45Å, respectively.

In Figure 4, we can see the micrographs by SEM of samples A-I, A-II and A-III calcined at 1100 °C, respectively. It is observed the average particle size of ferrite phase for the sample A-I, Figure 4a, of 1.2 µm, which is in agreement with that obtained by Rietveld refinement (1.03 µm).

The sample A-II, Figure 4b shows macro-aggregates containing small particles forming clusters. The image shows an agglomerated material with diffuse contours of particles having small average size with 0.1-0.8 µm (micrometric and nanometric particles) when calcined at 1100 °C/3h. By using the Rietveld method, was found average crystallite size of 0.61 ± 0.03 µm, thus having a relative correlation between SEM and XRD techniques. Due to the formation of macro-aggregates it is necessary to use high energy X-rays for accurate determination of the average particle size. Figure 4c shows an Ab-normal microstructure with grain size range of (0.3-2.0 µm). The arrows show an incomplete diffusion process caused by the lower mobility of the $Mn^{2+}$ ion during crystal growth.

Figure 5 shows the dependence of magnetization with the applied magnetic field by magnetic hysteresis for compositions A-I, A-II and A-III calcined at 350 °C/3h in air. The curves show hysteresis trend with low coercivities. The hystereses show soft magnetic materials. The magnetic parameters, i.e. of saturation magnetization, remnant magnetization and coercive field, obtained from the hysteresis are shown in Table 2. The sample A-II has the highest value of saturation magnetization of 33.2 $Am^2/kg$. The coercive field, ranging between 0.005 and 0.009 T, is higher for the sample A-I. According to the Rietveld refinement, the average crystallite size of the three samples are 17.69 (A-I), 16.81 (A-II), and 14.92 nm (A-III) when calcineds at 350 °C/3h, respectively. Very small particles below a critical size Dc, and not well defined, around 100 nm, show a sensitivity to magnetic fields [32]. The magnetization is explained by coherent rotation of magnetic moments. In the hysteresis of the sam-

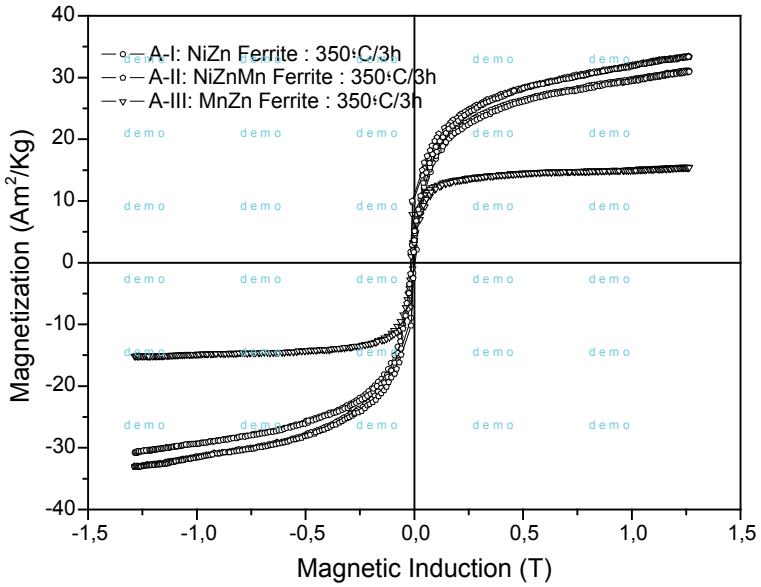


**Figure 5:** Hysteresis cycles of the composition of ferrites A-I, A-II and A-III, calcineds at 350 °C/3h.

**Table 2:** Magnetic properties for composition of A-I, A-II and A-III, calcineds at 350 °C/3h.

| Ferrite | *Ms ($Am^2/Kg$)* | *$M_R$ ($Am^2/Kg$)* | *$H_C$(T), Error. Max: ± 1.7 × $10^{-4}$* |
|---|---|---|---|
| A-I | 30.92 ± 2.82 | 5.57 ± 0.81 | 0.009 |
| A-II | 33.20 ± 2.97 | 4.09 ± 0.68 | 0.004 |
| A-III | 15.48 ± 1.82 | 2.95 ± 0.53 | 0.006 |

ples A-I and A-II, it is noted that the curves do not saturate even with a field strength above 1T.

The theoretical magnetization, for each ferrite is shown below. The values are calculated based on the magnetic contributions and the stoichiometric amount of each ion in the structure.

Unit cell of ferrite $Ni_{0.5}Zn_{0.5}Fe_2O_4$

Tetrahedral Position (4 $Zn^{2+}$ ions, 4 $Fe^{3+}$ ions), Octahedral Position (12 $Fe^{+3}$ ions, 4 $Ni^{+2}$ ions) M = 5 μB (12-4) 0 μB + (4) + 2 μB (4) = 48 μB/unit cell = 6 μB/cell.

Unit cell of ferrite $Ni_{0.2}Zn_{0.5}Mn_{0.3}Fe_2O_4$

Tetrahedral Position (4 $Zn^{2+}$ ions, 4 $Fe^{3+}$ ions), Octahedral Position (12 $Fe^{3+}$ ions, 1.6 $Ni^{2+}$ ions, 2.4 $Mn^{+2}$ ions) M= 5 μB (12-4) + 0 μB (4) + 2 μB (1.6) + 5 μB (2.4) = 55.2 μB/unit cell = 6.9 μB/cell.

Unit cell of ferrite $Mn_{0.5}Zn_{0.5}Fe_2O_4$.

Tetrahedral Position

(4 $Zn^{2+}$ ions, 4 $Fe^{3+}$ ions), Octahedral Position (12 $Fe^{3+}$ ions, 4 $Mn^{2+}$ ions) M = 5 μB (12-4) + 0 μB (4) + 5 μB (4) = 60 μB/unit cell = 7.5 μB/cell.

Figure 6 shows the hysteresis of A-I, A-II and A-III compositions calcineds at 1100 °C/3h. The data were observed in Table 3 with a high saturation magnetization of 86.05 $Am^2/kg$ for A-I ferrite. The XRD has shows a reduction of hematite phase and coincides with increasing magnetic property. Factors, such as chemical composition, homogeneity (synthesis) and energy diffusion of the ions in tetrahedral and octahedral positions are preponderant in this process [33]. There is an increase of coercivity of the sample A-III at 1100 °C/3h.

It was observed that the magnetization does not depend only on the quantity of spinel phase. Several factors alter the final effect of magnetization on ferrites. The higher theoretical magnetization in a unit cell, observed in the composition without nickel, does not imply a high magnetization of the bulk of the material. Factors such as: Single phase, added metal type, crystal size and imperfections are effects that alter the magnetization in the bulk. These factors alter the movement of the domain walls causing decreased magnetization. The microstructure of sample A-I shows particles of average size of 1 μm. Samples A-II and A-III, show small particle sizes around of big particles typical of Ab-normal microstructure. Competition in the

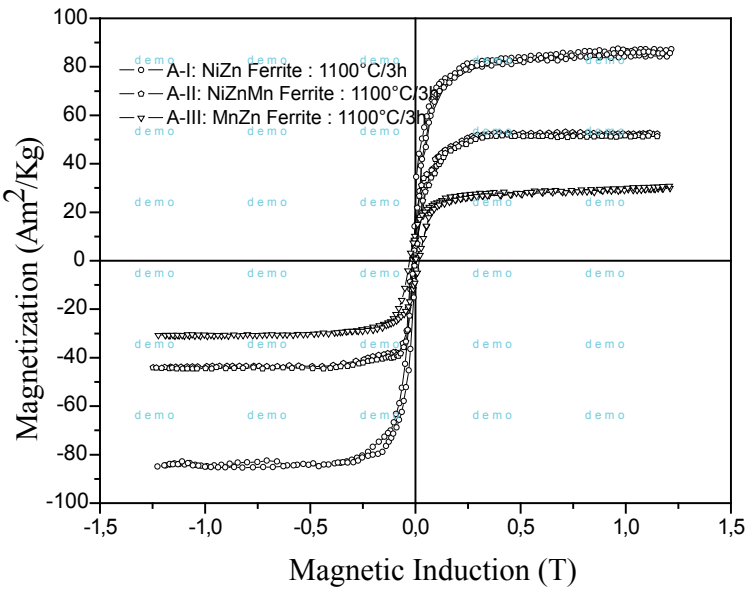


**Figure 6:** Hysteresis cycles of the composition of ferrites A-I, A-II and A-III calcineds at 1100 °C/3h.

**Table 3:** Magnetic properties of A-I, A-II and A-III compositions calcineds at 1100 °C/3h.

| Ferrite | $M_S$ ($Am^2/kg$) | $M_R$ ($Am^2/kg$) | $H_C$ (T), Er. Max: ± 6 × $10^{-4}$ |
|---|---|---|---|
| A-I | 86.05 ± 5.02 | 14.51 ± 1.61 | 0.008 |
| A-II | 48.26 ± 3.27 | 7.47 ± 1.27 | 0.008 |
| A-III | 30.75 ± 3.01 | 9.82 ± 2.11 | 0.02 |

diffusion process between the Ni and Mn ions causes a strong inhibition in grain growth (growth kinetics). The Bohr magneton increase due to the addition of Mn in NiZn ferrite is decompensated by inhibition of grain size. This effect limits the expansion of domains under the application of magnetic fields. The Mn ion can present states of $Mn^{+2}$ and $Mn^{+3}$, which facilitates the diffusion of the smaller ion [34]. This explains the lower homogeneity of the microstructure of sample A-III.

Figure 7 shows the saturation magnetization as a function of manganese concentration for different calcining temperatures in ferrite of formula $Ni_{0.5-x}Zn_{0.5}Mn_xFe_2O_4$. One can observe the decrease in magnetization with increasing manganese concentration. Occurs a reversal in the trend of the magnetization at 900 °C for AII compositions. Due to growth kinetics, larger particles have large domains volume and therefore get have greater magnetization. The ion $Fe^{3+}$ has a 3d5 configuration with five unpaired electrons, so does the $Mn^{2+}$ and $Mn^{3+}$ ions, having five and four unpaired electrons. The $Ni^{2+}$ and $Mn^{2+}/Mn^{3+}$ ions have a preference for octahedral positions but may occupy tetrahedral

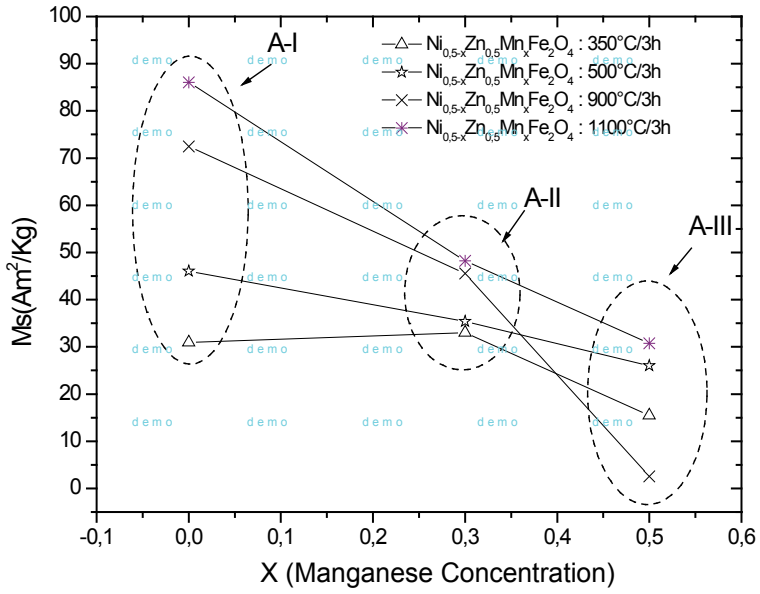


**Figure 7:** Saturation magnetization as a function of the x manganese concentration in $Ni_{0.5\,x}Zn_{0.5}Mn_xFe_2O_4$ ferrites calcineds at 350 °C, 500 °C, 900 °C and 1100 °C/3h.

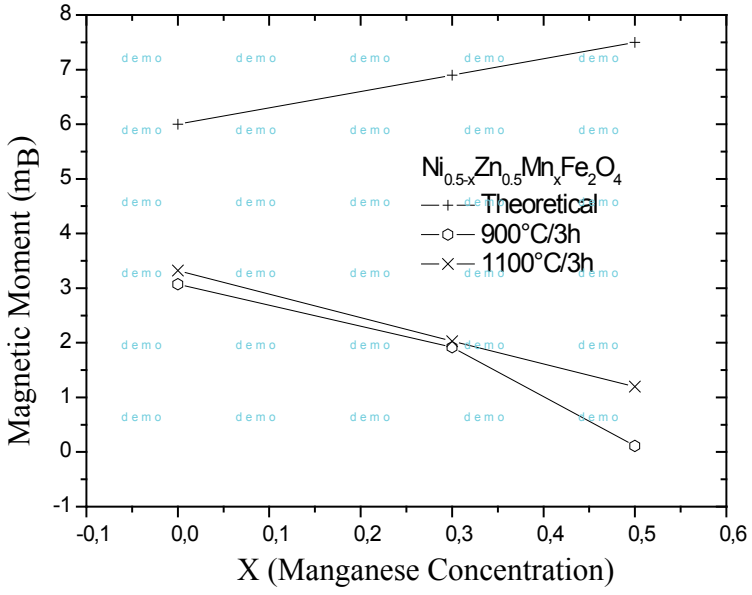


**Figure 8:** Magnetization in terms of magneton of Bohr per cell of $Ni_{0.5-x}Zn_{0.5}Mn_xFe_2O_4$ ferrite.

positions and form a mixed structure [35], while the $Zn^{2+}$ ions have a stronger binding energy to occupy tetrahedral positions.

It can be seen that increasing the concentration of Mn ions increases the theoretical magnetization. The theoretical values are obtained in experimental Bohr magnetons units. Equation 1 is used to calculate values of Bohr magnetons.

Figure 8 shows the theoretical and experimental magnetization in terms of the Bohr magneton. The theoretical magnetization is linear and increased with the addition of manganese. It is expected that the substitution of $Ni^{2+}$ ions by $Mn^{2+}$ ions will cause increases in magnetic parameters. However, the experiment shows that increasing $Mn^{2+}$ does not obey the calculation, the magnetization is decreased with increasing manganese concentration. This indicates that the Mn ion replaces partially the positions of $Fe^{+3}$ and forms a mixed spinel structure.

The magnetic measurements show that the Mn ion replaces the tetrahedral and octahedral positions and causes the magnetic property in the ferrite to decrease. The high concentration of the ion in the octahedral position (low spin) is that causes the decrease of the magnetization. The theoretical calculation is done as a function of the homogeneous distribution in high spin (tetrahedral) and low spins, but with manganese replacing the high spin positions.

The addition of $Ni^{+2}$ favors the inverse spinel structure, with the ion in sites B (octahedral positions), low spin, Figure 9. The low spin state causes the pairing of electrons in a position of lower energy and favors higher magnetic result due to $Fe^{+3}$ ions being in tetrahedral positions with a, high spin. The spinel structure with Ni at sites A (tetrahedral positions) shows that valence electrons in the low spin position have strong local magnetization and increase the vibrational state (phonons), with a lower demagnetizing effect. The interaction of electrostatic forces (chemical bonds) of Ni in the tetrahedral position favors the effect increase in the vibrational state increase (phonons). The Mn, when in octahedral positions B, is positioned in conditions of high stability. This phenomenon contributes less to the general vibrational state of the structure. This is observed with the increase of the lattice parameters with the concentration of Mn. This fact diminishes the effect of repulsion between the atomic orbitals of the ions in the chemical bonds. The remnant magnetization increased and the coercive field decreased. The concentration of $Mn^{2+} \rightarrow Mn^{3+}$ causes an increase in the concentration of electronic vacancies and changes the electronic conductivity. The electronic driving effect has an associated magnetic field. This effect, which depends on the concentration of vacancies, alters the mobility of the spins and favors the decrease in the coercive field.

Thus, the $Mn^{+2}$ in octahedral position (low spin) causes increase of the stability of the atomic

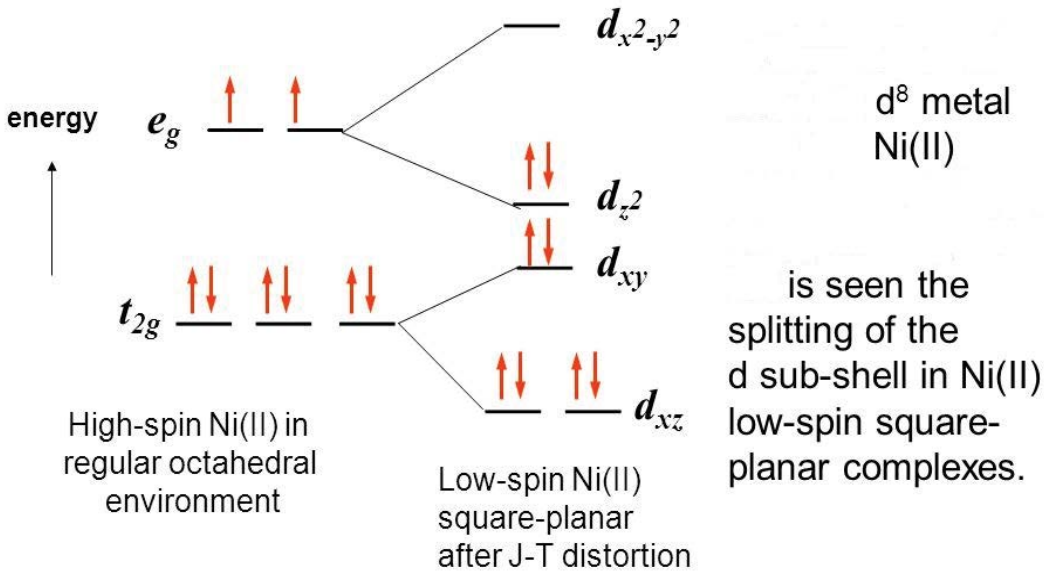


**Figure 9:** Diagram of energy for high-spin (regular octahedral position) and low-spin (regular tetrahedral position) of Ni(II).

**Table 4:** Theoretical magnetization, saturation magnetization, experimental magnetization in terms of magnetons of Bohr and the percentage of phase formed for the compositions calcineds at 900 °C and 1100 °C/3h.

| Temperature (°C) | Ferrites | Magneton of Borh ($\mu_B$) | $M_s$ ($Am^2/Kg$) | *M* (exp. In terms of $\mu_B$ (Eq. 1) | Phase % of ferrite |
|---|---|---|---|---|---|
| 900 | NiZn(A-I) | 6 | 72.37 ± 5.81 | 3.07 | 100 |
| | NiZnMn(A-II) | 6.9 | 45.55 ± 3.22 | 1.92 | 82 |
| | MnZn(A-III) | 7.5 | 2.55 ± 0.54 | 0.11 | 69 |
| 1100 | NiZn(A-I) | 6 | 86.05 ± 5.02 | 3.32 | 95 |
| | NiZnMn(A-II) | 6.9 | 48.26 ± 3.27 | 2.03 | 100 |
| | MnZn(A-III) | 7.5 | 30.75 ± 3.01 | 1.20 | 88 |

Percentage of Phases, Error: (Rw and Sig with precise parameters).

orbitals. Stability decreases the vibrational state of the atomic structure due to the phonons. The vibrational intensity of the structure (stretching of chemical bonds) directly influences the absorption of radiation from the material. Preliminary studies by MREI (the random-element-isodisplacement modified) conclude that this phenomenon is true.

Thus, the inverse spinel structure can promote a high increase in concentration of bivalent ions in octahedral positions, having low spin (positions B), with high energy electrons in the valence band (chemical bond). The interaction with 6 (six) neighboring atoms induces a strong absorption of radiation and change of vibrational state of the structure.

Table 4 shows that the Bohr magneton has an inverse tendency to experimental magnetization in terms of $\mu_B$. The percentage of the ferrite phase and the saturation magnetization defines the magnetic hysteresis performance. When calcined at a temperature of 1100 °C/3h the saturation magnetization is higher. When manganese is added, increases the magneton Bohr caused by the increase of pairs of unpaired electrons.

The change in the magnetic properties of NiZn ferrite with the substitution of $Ni^{2+}$ ions by $Mn^{2+}$ ions strongly depends of factors such as the solubility of the manganese in spinel lattice and the positions occupied by these cations in the tetrahedral and octahedral sites and of the grains size. That way these properties also depend heavily on intrinsic and extrinsic characteristics (synthesis and processing, additives, chemical homogeneity, structure and microstructure factors). The exchange interaction between ions of sites A and B increases as the interatomic distance decreases. The ionic radius of manganese is 16% higher than that the nickel radius and hampers the mobility in the lattice, which can cause variational distribution of Mn ions (~20% octahedral sites) and as a consequence decrease in magnetization [36]. A small concentration of $Mn^{3+}$ ions having an ionic radius near the $Ni^{2+}$ ion must occur. Due to the possible substitutions of these ions in different positions of the atomic structure, there are modifications in the electrostatic interactions, and stability, according to the positions occupied by the $Mn^{3+}$ ion. Above 700 °C there is a loss of weight due to the volatilization of zinc, this leading to the transfer of $Fe^{3+}$ ions in tetrahedral positions, which increases the cancellation of spins and decreases the magnetization. Other factors include the precipitation of hematite phase, which have antiferromagnetic property, the particle size and the volume of the magnetic domains.

Figure 10 shows the reflectivity curves as a function of frequency for samples A-I (NiZn ferrites) calcined at 1100 °C/3h in different thicknesses. The maximum attenuation is observed in sample with a thickness of 5.5 mm with an absorption of -16.01 dB (97.5%) in the 8.2 GHz region (starting in the X-band). It is not possible to observe the saturation of the attenuation of this material, which may have greater absorption at lower frequencies. Along the X-band the attenuation decreases to -1 dB. With a thickness of 5.0 mm the attenuation is -11.88 dB (93.5%) in the 8.7 GHz region. Decreasing the thickness to 4.0 mm leads to a decrease in the attenuation to -5.88 dB (74.17%), which decrease of 20.33% lower than for a thickness of 5.5 mm. However, the reduced attenuation shows a behavior of broadband absorber, maintaining the absorption in the X- band. Thickness of 5.5 mm and 5.0 mm show a narrow band absorber behavior, magnetic resonance occurs at a specific frequency. A thickness of 3.0 mm shows an attenuation of - 2.56 dB (44.5%), which remains unchanged

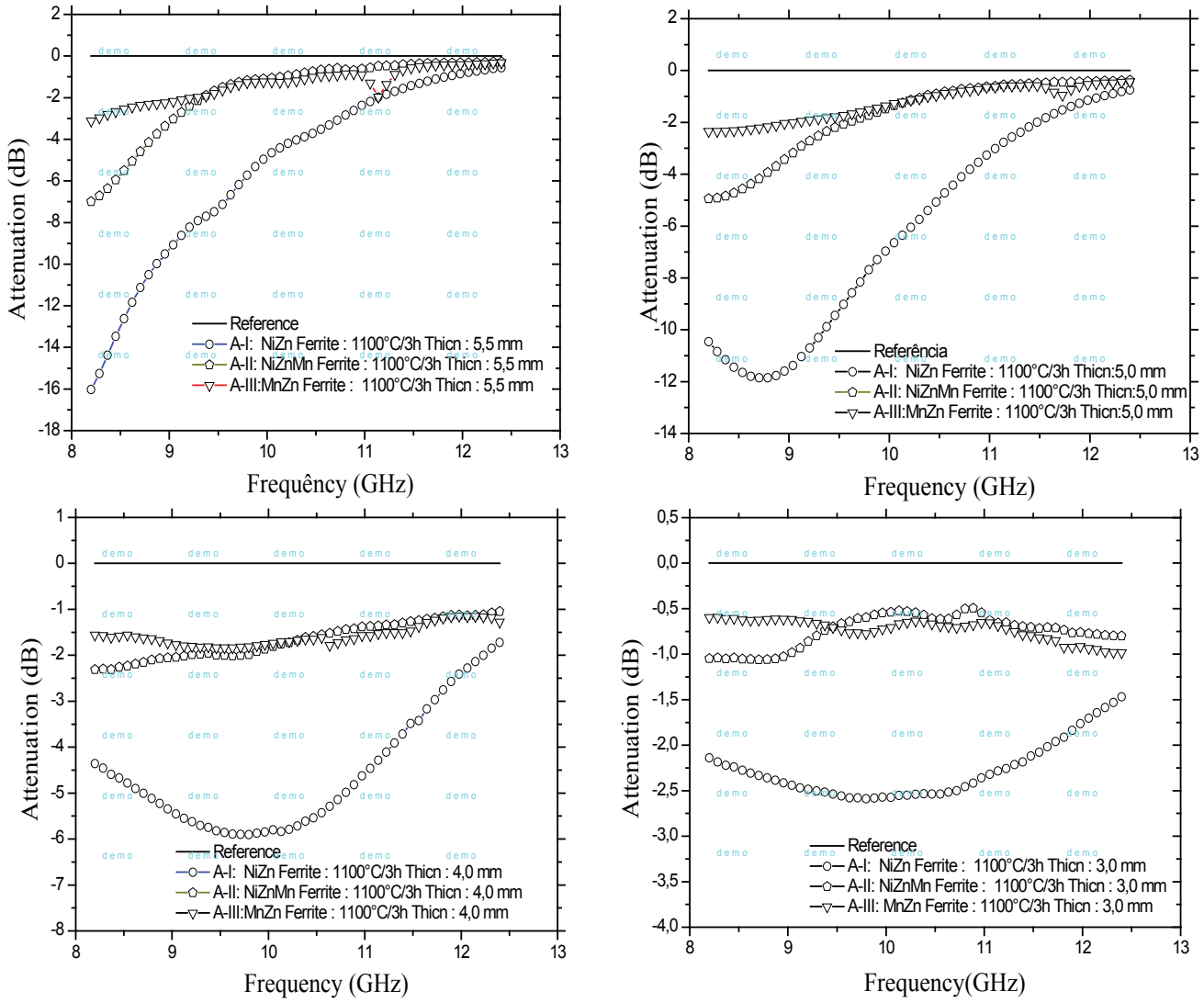


**Figure 10:** Comparison of the reflectivity curves of A-I, A-II and A-III compositions calcineds at 1100 °C/3h. Composites of Epoxy(araudite)/ferrite powders with thickness of 3.0, 4.0, 5.0 and 5.5 mm.

between 8.2 and 12.4 GHz. This observation shows that the average size of the larger grains causes the formation of multiple domains and increases the magnetization, interfering in the absorption characteristic of the material [27].

In Figure 10 it is shown that the polymer-ferrite composites with a thickness of 5.5 mm absorb electromagnetic radiation with more intensity. This is due to the absorption effect of the radiation by a greater number of ferrite particles and high dissipation of the waves by phonons in the crystals with absorption of heat by the interface of ferrite/ dielectric polymer.

The ability of the crystal to absorb the radiation and propagate the waves by phonons is intrinsically dependent on the capacity of the polymer to absorb some of the dissipated heat. Thus, it is clear that the dissipation is dependent on the amount of polymer in the composite. This is made clear by observing the variable characteristics of radiation absorption as a function of the thickness of the composites [28,29].

Table 5 shows that the efficiency of attenuation of the magnetic wave incident depends on the inverse factor of manganese addition in ferrites. The analysis shows that manganese does not contribute to an increase in reflectivity [37]. The A-I composition obtain better performs as an absorbing material, with 97.5% attenuation of the electromagnetic wave incident at 1100 °C/3h. Compositions A-II and A-III have attenuations of 80% and 50%, respectively. By correlating the reflectivity data, with the hysteresis curves obtained in the Rietveld analysis, it can be seen that the

**Table 5:** Comparison between different characteristics of A-I, A-II and A-III compositions calcineds at 1100 °C/3 h. Average Attenuation (dB), Absorption Incident Radiation (%), Saturation Magnetization (Ms), Cristal Size (µm).

| Composition | Average Attenn. (dB) | Absorption Inc. Rad. (%) | Ms ($Am^2/Kg$) | Cs (µm) |
|---|---|---|---|---|
| A-I | ~-16 | 98 | 86.05 ± 5.02 | 1.03 |
| A-II | ~-7 | 80 | 48.26 ± 3.27 | 0.61 |
| A-III | ~-3 | 50 | 30.75 ± 3.01 | 1.14 |

Comparative scale of reflectivity data.

percentage of absorption radiation increased with saturation magnetization. As already explained the crystal size influences the quantity and average volume of magnetic domains. These factors, with the percentage of ferrite phase, increase the radiation absorption of these composites.

The incident radiation alters the phonons in the crystals and promotes electrons to states of energy that overcome the gap, valence band/ conduction band. The effect of the absorption of radiation and energy dissipation depends on the phonon-electron dualism. Infrared light absorption causes multiphonon relaxation. The upcoming thermal radiation in wavelength depends of chemical bond characteristics inside the crystals (general vibrational state of structure) [38]. The total contribution of heat propagation is the sum of the contributions of electrons and phonons. The main contribution is made by phonons. The conduction of heat caused by electrons increases with the temperature of the composite. The rate, frequency and time of radiation exposure changes the maximum heating effect of the crystals. In order to increase the population of electrons in the conduction band, the energy must be high (~1.9 eV) due to positioning above the Fermi level. This implies radiation with lower wavelength, such as ultraviolet. The magnetic crystals dispersed in the dielectric polymer have limited electronic mobility because the electrons get trapped in the crystals. This random electronic conductivity also causes thermal conductivity. The crystal-polymer interaction limits the conductivity to polymers in contact with the crystals which reduces the heat propagation on the surface of the crystals and causes local effect of nanodegradation. This explains the factor limiting the size of the crystals, the dispersion in the polymer and the thickness of the polymer-crystal composites. The catastrophic effect of increasing the incidence of radiation in cycles causes demagnetization of the surface towards the interior of the crystal. Therefore, the efficiency of the magnetic effect on absorption decreases as a function of time.

In our work nanometric particles did not show a direct correlation between the Bohr-magneton and the absorption of radiation. A higher saturation magnetization does not show high Bohr magneton. An analysis of the particle size indicates that the low number of unit cells with coherent magnetization in small particles causes the decrease in the absorption of incident radiation. This can be seen in Table 5 where the composition with 100% ferrite phase and particles smaller than 1 µm shows less absorption relative as compared to the composition with 95% ferrite phase and particles with an average size of 1 µm.

## Conclusions

It was concluded that the saturation magnetization coincides with increasing absorption of radiation. However, the calculated Bohr magneton showed an inverse tendency on the Ms. The nanometric particle size limits the effect of the absorption of radiation due to the small bulk with a low number of unit cells with coherent magnetization. This indicates that in micrometric particles, is important the formation of multi-domain to the effect for absorption of radiation and an approach with the calculated magneton of Bohr in ferrites. The results demonstrate that in nanometric particles in the absence of multi-domain, high concentrations of imperfections on the bulk and on the surface cause deviations between the calculated Bohr magneton and the experimental magnetization, however, yet presents high absorption capacity of the radiation that depends on the movement of electrons in the crystal and the propagation of the waves by phonons in the atomic and polymer structure. Thus, factors such as the metals forming the atomic structure and the size of the crystals and the thickness of the polymer-crystal composite are predominant factors in the absorption of radiation.

## References

1. M Sugimoto (1999) Low-temperature synthesis of

nanosized NiZn ferrite. J Am Ceram Soc 82: 269-280.

2. AM Gama, MC Rezende, CC Dantas (2011) Dependence of microwave absorption properties on ferrite volume fraction in MnZn ferrite/rubber radar absorbing materials. J Magn Magn Mater 323: 2782-2785.

3. UR Lima, MC Nasar, RS Nasar, JH Araújo, MC Rezende (2008) NiZn nanoferrite for radar-absorbing materials. J Magn Magn Mater 320: 1666-1670.

4. Y Yamamoto, A Makino, T Yamaguchi, I Sasada (1997) Fine grained ferrite for low profile transformer. IEEE Trans Magn 33: 3742-3744.

5. T Kasahara, D Shindo, H Yoshikawa, T Sato, K Kondo (2007) In situ observations of domains structures and magnetic flux distributions in Mn-Zn and Ni-Zn ferrites by Lorentz microscopy and electron holography. J Elect Micr 56: 7-16.

6. G Mathubala, A Manikandan, S Arul Antony, P Ramar (2016) Photocatalytic degradation of methylene blue dye and Magneto-optical studies of magnetically recyclable spinel $Ni_xMn_{1-x}Fe_2O_4$ (x = 0.0-1.0) nanoparticles. J Molec Struct 1113: 79-87.

7. A Manikandan, M Durka, K Seevakan, S Arul Antony (2015) A novel one-pot combustion synthesis and opto-magnetic properties of magnetically separable spinel $Mn_xMg_{1-x}Fe_2O_4$ ($0.0 \leq x \leq 0.5$) nanophotocatalysts. J Supercon Nov Magn 28: 1405-1416.

8. MV Vasic, B Antic, A Kremenovic, AS Nikolic, M Stoiljkovic, et al. (2006) Zn, Ni ferrite/NiO nanocomposite powder obtained from acetylacetonato complexes. Nanotech 17: 4877-4884.

9. P Yadoji, R Peelamedu, D Agrawal, R Roy (2003) Microwave sintering of Ni-Zn ferrites: Comparison with conventional sintering. Mater Sci Eng B 98: 269-278.

10. UR Lima, MC Nasar, RS Nasar, JH Araújo, MC Rezende, et al. (2008) Synthesis of NiCuZn ferrite nanoparticles and microwave absorption characterization. Mater Sci Eng B 151: 238-242.

11. IC Nlebedim, AJ Moses, DC Jiles (2013) Non-stoichiometric cobalt ferrite $Co_xFe_{3-x}O_4$ (x = 1.0 to 2.0): Structural, magnetic and magnetoelastic properties. J Magn Magn Mater 343: 49-54.

12. D Ravinder, K Latha (1999) Dielectric behaviour of mixed Mg-Zn ferrites at low frequencies. Mater Lett 41: 247-253.

13. Amarendra K Singh, Ajay Verma, OP Takur, Chandra Prakash, TC Goel, et al. (2003) Electrical and magnetic properties of Mn-Ni-Zn ferrites processed by citrates precursor method. Mater Lett 57: 1040-1044.

14. Vuk Uskokovic, Miha Drofenik (2005) A mechanism for the formation of nanostructured NiZn ferrites via a microemulsion-assisted precipitation method. Colloids Surf A Physicochem Eng Asp 266: 168-174.

15. LN Murthy, IV Kasi Viswanath, T Kondala Rao, Rajendra Singh (2009) Synthesis and characterization of Nickel copper ferrite. International Journal of ChemTech Research 1: 1308-1311.

16. Irena Szczygiel, Katarzina Winiarska (2014) Synthesis and characterization of manganese-zinc ferrite obtained by thermal decomposition from organic precursors. Journal of Thermal Analysis and Calorimetry 115: 471-477.

17. H Jun, Y Mi (2005) Preparation of high-permeability NiCuZn ferrite. J Zhejiang Univ Sci B 6: 580-583.

18. Y Köseoglu, MIO Oleiwi, R Yilgin, AN Kocbay (2012) Effect of chromium addition on the structural, morphological and magnetic properties of nano-crystalline cobalt ferrite system. Ceram Int 38: 6671-6676.

19. TT Ahmed, IA Rahman, SAM Tofail (2004) Effect of copper ion distribution on the magnetization of nanoscaled NiZn ferrite. J Magn Magn Mater 272-276: 2250-2252.

20. SC Byeon, KS Hong, H Je (1997) Oxygen partial pressure dependent magnetic properties of manganese-zinc ferrite polycrystals. Mater Res Bull 32: 579-588.

21. A Thakur, M Singh (2003) Preparation and characterization of nanosize $Mn_{0.4}Zn_{0.6}Fe_2O_4$ ferrite by citrate precursor method. Ceram Int 29: 505-511.

22. EE Sileo, RR Rotelo, SE Jacobo (2002) Nickel zinc ferrites prepared by the citrate precursor method. Physica B: Cond Matter 320: 257-260.

23. A Manikandan, J Judith Vijaya, L John Kennedy, M Bououdina (2013) Structural, optical, and magnetic properties of $Zn_{1-x}Cu_xFe_2O_4$ nanoparticles prepared by microwave combustion method. J Molec Struct 1035: 332-340.

24. A Manikandan, L John Kennedy, M Bououdina, J Judith Vijaya (2014) Synthesis, optical and magnetic properties of pure and Co-doped $ZnFe_2O_4$ nanoparticles by microwave combustion method. J Magn Magn Mater 349: 249-258.

25. LC Folgueras, MA Alves, MC Rezende (2014) Evaluation of a microstructured microwave absorbent coating applied to a glass fiber/ polyphenylene sulfide laminated composite. Mat Res 17: 197-202.

26. E Rezlescu, L Sachelarie, PD Popa, N Rezlescu (2000) Effect of substitution of divalent ions on the electrical and magnetic properties of Ni-Zn-Me ferrites. IEEE Trans Magn 36: 3962-3967.

27. Kyoung-Sik Moon, CP Wong, Soo-Hyung Kim, Hyung Dochoi, Seung Han, et al. (2007) Ferrite polymer composite for improving the electromagnetic compatibility of semiconductor packaging. J Elect Mater 36: 1711-1718.

28. NE Kazantseva, J Vilkakova, V Kresalek, P Saha, I Sapurina, et al. (2004) Magnetic behaviour of composites containing polyaniline-coated manganese-zinc ferrite. J Magn Magn Mater 269: 30-37.

29. R Dosoldil, M Usakova, J Franek, J Slava, A Gruskova (2010) Particle size and concentration effect on permeability and EM-wave absorption properties of hybrid ferrite polymer composites. IEEE Transactions on Magnetics 46: 436-439.

30. MP Pechini (1967) Method of preparing lead and alkaline earth titanates and niobates and coating method using the same to form a capacitor. US PATENT.

31. M Chaitanya Varna, GSVRK Choudary, A Mahesh Kumar, KH Rao (2014) Estimating the cátion distribution in $Ni_{0.65-x}Zn_{0.35}Co_xFe_2O_4$ ferrites using X-ray, FT-IR, and magnetization measurements. Phys Res Int 2014: 1-9.

32. Georgia C Papaefthymiou (2009) Nanoparticle magnetism. Nano Today 4: 438-447.

33. R Nongjai, S Khan, K Asokan, H Ahmed, I Khan (2012) Magnetic and electrical properties of in doped cobalto ferrite nanoparticles. J App Phys 112: 084321.

34. I Maria, K Dzmitry, P Vladimir, F Yulia (2009) Structure and magnetic properties of Mn-Zn ferrites. Proceedings of Symposium I, ¨Multifunctional Advances Composites Materials: Manufacturing, Structure, Properties¨, E-MRS, Warsaw, Poland, 14-18.

35. D Carta, MF Casula, A Falqui, D Loche, G Mountjoy, et al. (2009) A structural and magnetic investigation degree in ferrites nanocrystals $MFe_2O_4$(M = Mn, Co, Ni). J Phys Chem C 113: 8606-8615.

36. C Venkataraju (2009) Effect of nickel on the structural properties of Mn Zn ferrite nano particles. Appl Phys Res 1: 41-45.

37. JEM Silva, RS Nasar, MC Nasar, CL Firme, JH Araújo (2015) Correlation between coercive field and radiation attenuation in Ni and Mg ferrite doped with Mn and Co. J Magn Magn Mater 394: 274-279.

38. TT Basiev, Yu V Orlovskii, KK Puhhov, F Auzel (1997) Multiphonon relaxation of the electronic excitation in optical crystals doped with rare-earth ions. Laser Physics 7: 1139-1152.

ISSN 2631-5068